Available online at www.sciencedirect.com

ScienceDirect

Ceramics International 40 (2014) 1423–1429

CERAMICS INTERNATIONAL

www.elsevier.com/locate/ceramint

Fabrication of WO_3 nanotube sensors and their gas sensing properties

Soyeon An, Sunghoon Park, Hyunsung Ko, Chongmu Lee*

Department of Materials Science and Engineering, Inha University, 253 Yonghyun-dong, Nam-gu, Incheon 402-751, Republic of Korea

Received 18 April 2013; received in revised form 17 June 2013; accepted 4 July 2013
Available online 18 July 2013

Abstract

WO_3 nanotubes were synthesized using TeO_2 nanowire templates. Transmission electron microscopy revealed the nanotubes to have tube diameters, lengths, and wall thicknesses ranging from 100–200 nm, 3–4 μm, and 20–30 nm, respectively. The multiple networked WO_3 nanotube sensors showed responses of 144–677% in the NO_2 concentration range of 1–5 ppm at 300 °C. These responses were approximately double those observed for the WO_3 nanorod sensors over the same NO_2 concentration range. A model describing the gas sensing mechanism of WO_3 NTs is also proposed.

Keywords: WO_3 nanotubes; Gas sensors; Response; NO_2

1. Introduction

One-dimensional (1D) nanostructure-based sensors have the advantages of higher sensitivity, superior spatial resolution, and rapid response due to the high surface-to-volume ratios than thin film gas sensors [1–3]. Over the past two decades, considerable efforts have been made to synthesize metal-oxide 1D nanostructures such as nanowires, nanorods, nanobelts, and nanoribbons and to investigate their gas sensing properties [4]. On the other hand, there have been few reports on nanotube gas sensors compared to other 1D nanostructures.

Tungsten oxide (WO_3) is an important n-type semiconducting material with a band gap of 2.7 eV, with applications in gas sensing, photocatalysis, and electrochromic devices [5]. Gas sensors based on WO_3 nanostructures have attracted considerable attention because of their excellent sensitivity and selectivity in detecting a range of gases [6,7]. WO_3 nanowires or nanorods have exhibited favorable sensing properties to NO_2, H_2S, O_3, H_2, NH_3, and liquefied petroleum gas at elevated temperatures (200–300 °C) [8–12]. On the other hand, little is known regarding the synthesis and gas sensing properties of WO_3 nanotubes (NTs) [13] in spite of their advantage of higher surface-to-volume ratios than WO_3 nanowires or nanorods. This paper reports the synthesis, structure and NO_2 gas sensing properties of WO_3 NTs. A model describing the gas sensing mechanism of WO_3 NTs is also proposed.

2. Experimental

WO_3 nanotubes were synthesized using a TeO_2 nanowire template. First, TeO_2 nanowires were synthesized by the thermal evaporation of Te powders on Si (100) substrates. Approximately 2.0 g of Te powders was placed in an alumina crucible and located at the center of a horizontal quartz tube, which was mounted inside a conventional horizontal tube furnace. During nanowires synthesis, the temperature of the source materials was maintained at 500 °C for 1 h. After synthesis, the furnace was cooled to room temperature and the Si substrate was removed from the tube. The TeO_2 nanowires were then transferred to a sputter chamber to coat them with a WO_3 thin film. The sputter deposition of WO_3 was conducted at 50 W in an Ar atmosphere at an Ar flow rate of 10 sccm for 10 min. Throughout the sputtering process, the Si substrate was rotated for more uniform coating of WO_3 on the surface of the TeO_2 nanorods. The pressure in the reactor was maintained at 20 mTorr. The WO_3

*Corresponding author. Tel.: +82 32 860 7536; fax: +82 32 862 5546.
E-mail address: cmlee@inha.ac.kr (C. Lee).

0272-8842/$ - see front matter © 2013 Elsevier Ltd and Techna Group S.r.l. All rights reserved.
http://dx.doi.org/10.1016/j.ceramint.2013.07.025

nanotubes were synthesized by eliminating the TeO_2 core by thermal evaporation at 700 °C in air for 1 h at 1 mTorr pressure. A selective elimination of TeO_2 is possible by heating the TeO_2-core/WO_3-shell nanostructures at a high temperature because of a big difference in melting point between the two materials (TeO_2 (732 °C) and WO_3 (1,473 °C)). TeO_2 evaporates at a lower temperature than WO_3 (1,473 °C) because of this big difference in melting point. Actually, the temperature increases, TeO_2 nanowires started to evaporate at ~550 °C, whereas the evaporation of the WO_3 shell layers occurred above 900 °C. As a result of the selective elimination of TeO_2, we obtained WO_3 nanotubes. On the other hand, the WO_3 nanorods were synthesized by the thermal evaporation of WO_3 powders on Si (100) substrates in an N_2 atmosphere at 1,100 °C at 1 Torr for 1 h.

The collected WO_3 1D nanostructure samples were characterized by scanning electron microscopy (SEM, Hitachi S-4200), transmission electron microscopy (TEM, Philips CM-200) equipped with an energy-dispersive X-ray spectrometer (EDXS) and X-ray diffraction (XRD, Philips X′pert MRD diffractometer). The crystallographic structure was determined by glancing angle XRD with Cu K_α radiation (0.15406 nm), a scan rate of 4°/min, a 0.5° glancing angle, and a rotating detector.

For the sensing measurement, Ni (~10 nm) and Au (~50 nm) thin films were deposited sequentially by sputtering to form electrodes using an interdigital electrode (IDE) mask. Multiple networked WO_3 1D nanostructure gas sensors were fabricated by pouring a few drops of the WO_3 1D nanostructures-suspended in ethanol onto the oxidized Si substrates equipped with a pair of IDEs with a gap length of 20 μm. The electrical and gas sensing properties of the as-synthesized WO_3 1D nanostructures were measured using a home-built computer-controlled characterization system consisting of a test chamber, sensor holder, Keithleysourcemeter-2612, mass flow controllers and data acquisition system (Fig. 1). During the measurements, the 1D nanostructured gas sensors were placed in a sealed quartz tube with an electrical feed through. The test gas was mixed with dry air to achieve the desired concentration and the flow rate was maintained at 200 standard cubic centimeters per minute (sccm) using mass flow controllers. The working temperature of the sensors was adjusted by changing the voltage across the heater side. The gas sensing properties of the 1D nanostructure gas sensors were measured at 300 °C in a quartz tube placed in a sealed chamber with an electrical feed through. A set amount of NO_2 (> 99.99%, 1–5 ppm) gas was injected into the testing tube through a microsyringe, and the output voltage across the sensor in the nanotubes was monitored. The resistance of the sensor in dry air or in the test gas was measured from this voltage. The response of the 1D nanostructure sensors is defined as R_g/R_a for NO_2, where R_a and R_g are the electrical resistances of the sensors in air and target gas, respectively. The response time was defined as the time needed for the change in electrical resistance to reach 90% of the equilibrium value after injecting the gas. The recovery time was defined as the time needed for the sensor to return to 10% of the original resistance in air after removing the gas.

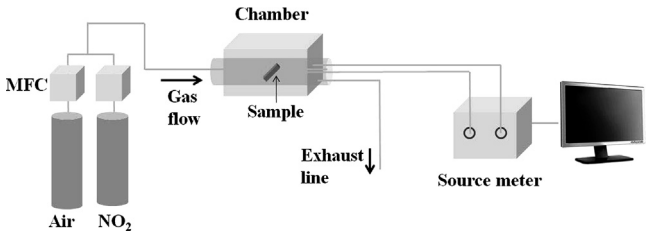

Fig. 1. Schematic diagram of the gas sensing measurement system.

3. Results and discussion

Fig. 2 and inset in Fig. 2 show SEM and enlarged SEM images of the WO_3 nanotubes prepared using a TeO_2 nanowire template. The specific surface area of the WO_3 nanotubes and WO_3 nanorods measured using the Brunauer–Emmet–Teller (BET) method was 67.7 and 21.4 m^2/g, respectively, suggesting that nanotubes have far larger surface area than nanorods. We can see many WO_3 nanoparticles in addition to WO_3 nanotubes in the SEM image. We surmise the nonuniform shape is due to the somewhat low substrate temperature in the thermal evaporation process for the synthesis of WO_3 nanotubes. If we had increased the substrate temperature a little bit, we could have obtained WO_3 nanotubes with a more uniform shape. The tube diameters and wall thicknesses of the nanotubes ranged from 100 to 120 nm and 20–30 nm, respectively as shown in the low-magnification TEM image (Fig. 3(a)). Fig. 3(b) presents a local high-resolution TEM (HRTEM) image of a nanotube. The resolved spacings between two neighboring parallel fringes in the image corresponding to the primitive monoclinic WO_3 (200) and (002) planes were approximately 0.37 and 0.39 nm. Fig. 3(c) shows the corresponding selected area electron diffraction (SAED) pattern of WO_3. The strong reflection spots in the corresponding selected area electron diffraction (SAED) pattern were assigned to the reflections of

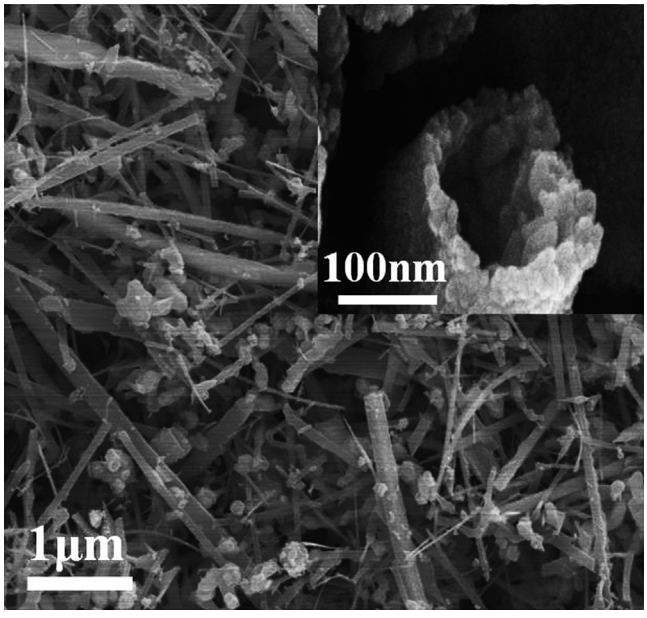

Fig. 2. SEM image of the WO_3 nanotubes. Inset, enlarged SEM image of a typical WO_3 nanotube.

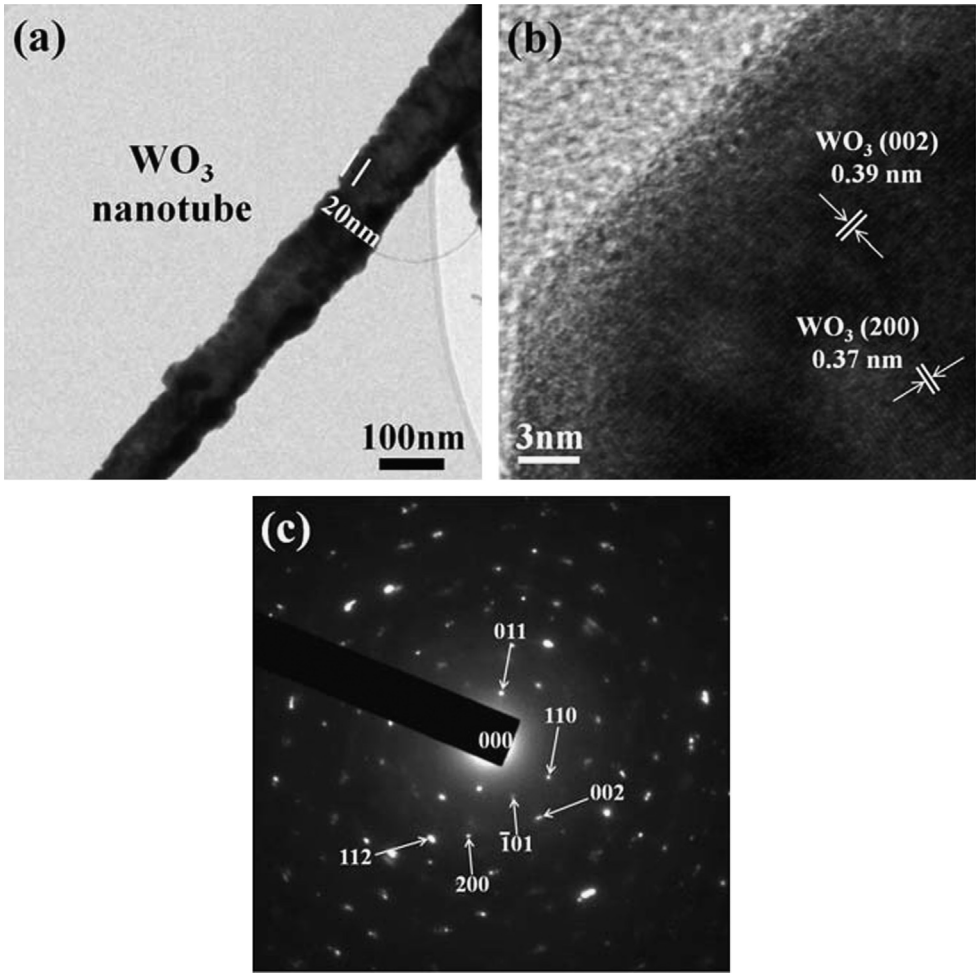

Fig. 3. (a) Low magnification TEM image, (b) high resolution TEM image, and (c) selected area electron diffraction pattern of the WO_3 nanotubes.

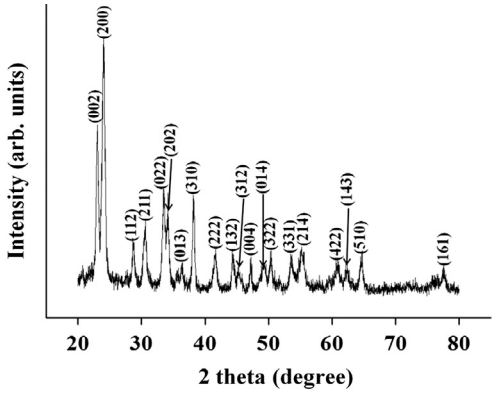

Fig. 4. XRD patterns of the WO_3 nanotubes.

primitive monoclinic-structured WO_3 with lattice constants $a=0.7327$ nm, $b=0.7564$ nm, $c=0.7727$ nm, and $\beta=90.488^\circ$, (JCPDS no. 89-4476). On the other hand, a close examination of the SAED pattern indicated that the reflection spots did not belong to the same zone axis, suggesting that the WO_3 nanotube in the TEM image is polycrystalline.

The XRD patterns of the WO_3 nanotubes also showed that the tubes were crystalline (Fig. 4). The reflection peaks in the XRD pattern of the WO_3 nanotubes were assigned to the (002), (200), (112), (211), (022), (202), (013), and (310) reflections of primitive monoclinic-structured WO_3 (JCPDS no. 89-4476). EDXS confirmed that the WO_3 nanotubes were composed of W and O (Fig. 5(a)). The Cu in the spectrum was attributed to the TEM grid. EDXS analyses (Fig. 5(b)) also confirmed that WO_3 nanotubes were synthesized successfully by showing higher W and O concentrations at both edge regions of the nanostructure.

Fig. 6(a) shows the dynamic responses of the WO_3 nanorods and WO_3 nanotubes to NO_2 gas in a range of 1–50 ppm at 300 °C. The resistance increased upon exposure to NO_2 and recovered completely to the initial value upon the removal of NO_2. The sensor responses to NO_2 gas were quite stable and reproducible for repeated test cycles. Fig. 6(b) and (c) shows an enlarged part of the data in Fig. 6(a) measured at a NO_2 concentration of 5 ppm for the WO_3 nanorods and WO_3 nanotubes, respectively, to reveal the moments of gas input and gas stop. The WO_3 nanorods showed responses of approximately 142, 175, 220, 272, 326, 383 and 462% at NO_2 concentrations of 1, 2, 3, 4, 5, 10 and 50 ppm, respectively (Table 1). On the other hand, the WO_3 nanotubes showed responses of approximately 144, 187, 338, 520, 677, 881 and 1,054% at NO_2 concentrations of 1, 2, 3, 4, 5, 10 and 50 ppm, respectively (Table 1). Therefore, the responses of the WO_3 nanotubes were approximately double

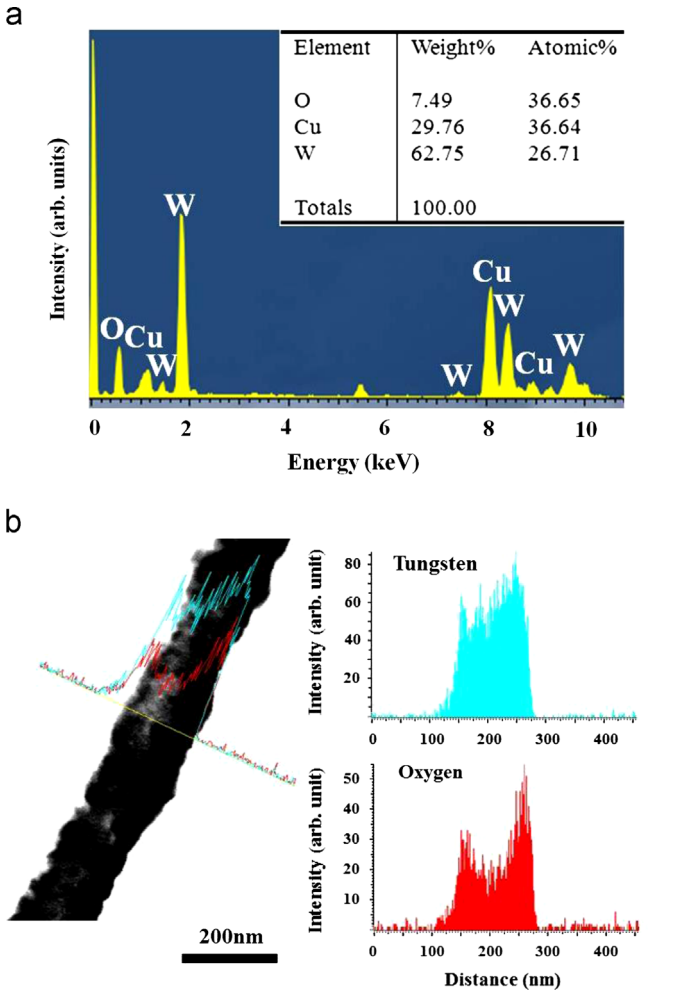

Fig. 5. (a) EDXS line scanning concentration profiles and (b) EDX spectra of the WO_3 nanotubes.

those of the WO_3 nanorods at 1–5 ppm NO_2. Fig. 6(d) shows the responses of the WO_3 nanorods and WO_3 nanotubes as a function of the NO_2 concentration. The response of an oxide semiconductor is commonly expressed as $R=A[C]^n+B$, where A and B are constants, n, and $[C]$ are exponent, and the target gas concentration, respectively [14]. Data fitting gave $R=46.420[C]+87.676$ and $R=139.753[C]+46.027$ for the WO_3 nanorod and WO_3 nanotube sensors, respectively. The responses of the nanotube sensor tends to increase more rapidly than that of the nanorod sensor as the NO_2 gas concentration was increased, suggesting that the response of the former would be far higher than that of the latter at high NO_2 gas concentrations such as a few thousand ppm NO_2, even though the response of the nanotubes were examined only in the NO_2 concentration range of 1–5 ppm. Table 1 also shows that the response and recovery times of the WO_3 nanotubes are considerably shorter than those of the WO_3 nanorods. The higher sensing speed of the nanotubes than the nanorods might also be attributed to the larger number of carriers generated at the larger surface of the nanotubes.

Table 2 [15–24] shows that the response of the WO_3 nanotubes was superior to those of typical semiconductor oxide 1D nanostructures such as SnO_2 nanobelts, ZnO nanorods, In_2O_3 nanowires, and MoO_3 lamellae and oxide semiconductor 1D heterostructures such as SnO_2-core/ZnO-shell nanofibers to NO_2 gas reported previously as well as that of WO_3 nanowires even though a somewhat higher NO_2 gas concentration range used in this study was considered. Although Table 2 suggests that the response of TiO_2 nanofibers is inferior to that of WO_3 nanotubes, the response for the TiO_2 nanofibers was measured at a far higher NO_2 concentration (200 ppm). An extrapolation of the response curve of the WO_3 nanotubes in Fig. 5(d) to 200 ppm would give a response of 252,400%. Therefore, the response of the WO_3 nanotubes is also higher to that of TiO_2 nanofibers.

Besides the responses to NO_2 gas, we also measured the responses of both WO_3 nanotubes and WO_3 nanorods to CO, C_2H_5OH and NH_3 to examine the selectivity of the two different WO_3 nanostructure sensors. Fig. 7 compares the responses of WO_3 nanotubes and WO_3 nanorods to those four different gases. The results reveal that both WO_3 nanotubes and WO_3 nanorods are more sensitive to NO_2 gas than other gases and that WO_3 nanotubes have a higher selectivity than WO_3 nanorods. Therefore, we may say that the sensors have particularly good selectivity for NO_2 gas.

The NO_2 gas sensing mechanism of the WO_3 nanotube sensor was modeled using the surface-depletion model [25], as shown in Fig. 8. Upon exposure to NO_2 gas, NO_2 gas adsorbs on the WO_3 nanotubes and electrons are released from the nanotubes, and are attracted to the adsorbed NO_2 molecules because an oxidizing gas, such as NO_2, acts as an electron acceptor, as shown in the following reactions [26]:

$$NO_2(g)+e^- \leftrightarrow NO_2^-(ads) \quad (1)$$

$$NO_2(g)+e^- \leftrightarrow NO(g)+O^-(ads) \quad (2)$$

As a result of these reactions, a depletion region forms in the surface region of each the WO_3 nanotube, resulting in an increase in the resistance of the nanotube sensor. On the other hand, after the NO_2 gas supply is stopped, the trapped electrons are released to the WO_3 nanotubes by NO_2 gas, leading to a decrease in the depletion layer width (Fig. 8) and resistance. This results in an increase in carrier concentration in the WO_3 nanotubes and a decrease in the surface depletion layer width. In other words, the removed electrons are returned to the conduction band, which results in a sharp decrease in electrical resistance in the WO_3 nanotube sensors.

The higher response of the WO_3 nanotube sensor than the WO_3 nanorods might be due to the higher surface-to-volume ratio of the WO_3 nanotubes. WO_3 nanotubes have a higher surface-to-volume ratio than WO_3 nanorods because of the large inner and outer surface, whereas WO_3 nanorods have only outer surfaces. A larger surface would lead to the release of a larger number of electrons from the nanostructure sensor upon exposure to NO_2 gas and collect a larger number of electrons in the nanostructure sensor after stopping the NO_2 gas supply. Therefore, a larger surface would result in a stronger response to NO_2 gas.

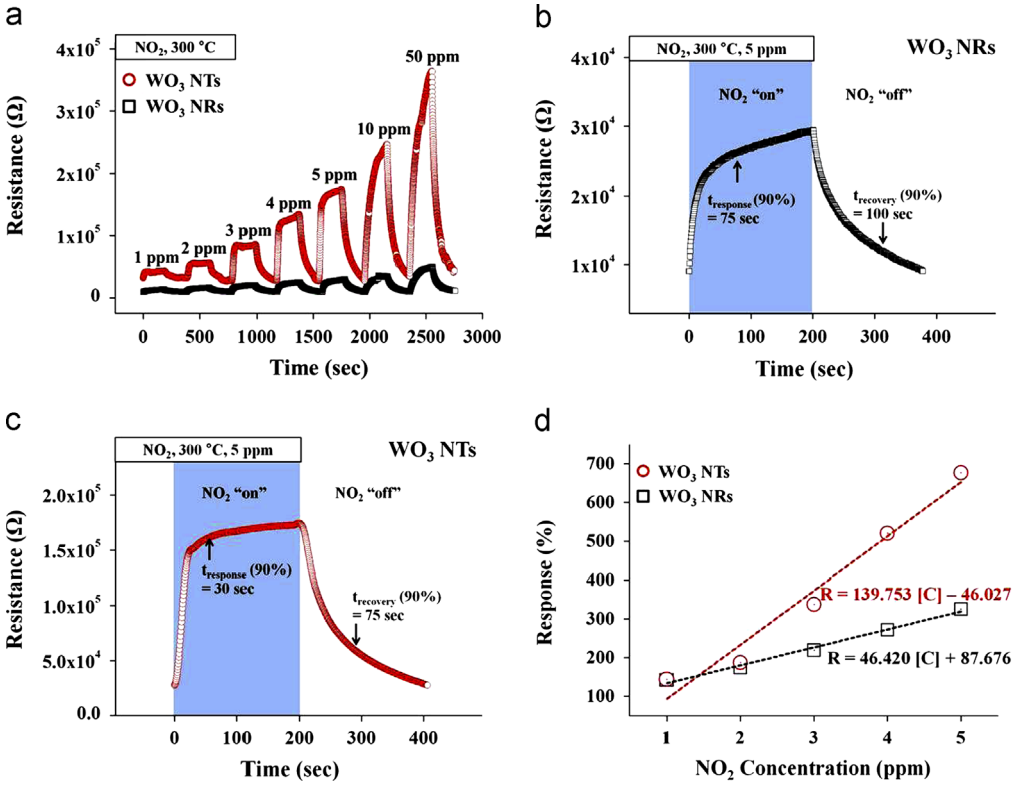

Fig. 6. (a) Dynamic responses of WO_3 nanorods and WO_3 nanotubes. (b) Enlarged part of the WO_3 nanorods curve in Fig. 6(a) at 5 ppm NO_2. (c) Enlarged part of the WO_3 nanotubes curve in Fig. 6(a) at 5 ppm NO_2. (d) Responses of the WO_3 nanorods and WO_3 nanotubes as a function of the NO_2 gas concentration.

Table 1
Responses, response times, and recovery times measured at different NO_2 concentrations for the WO_3 nanorods and WO_3 nanotubes at 300 °C.

NO_2 conc. (ppm)	Response (%)		Response time (s)		Recovery time (s)	
	WO_3 NRs	WO_3 NTs	WO_3 NRs	WO_3 NTs	WO_3 NRs	WO_3 NTs
1	142.31	144.45	100	20	100	70
2	174.85	186.98	85	20	120	85
3	219.54	337.89	80	15	110	100
4	272.29	520.27	80	40	120	90
5	325.69	676.57	75	30	100	75
10	382.85	881.41	110	90	90	70
50	462.40	1053.80	120	100	100	70

Table 2
Comparison of the response of the WO_3 nanotube sensor with those of other 1D nanostructured sensors reported previously.

Nanomaterial	NO_2 conc. (ppm)	Response (%)	Reference
WO_3 nanotubes	5	677	Present work
ZnO nanorods	0.1	40	[15]
SnO_2 nanobelts	0.3	230	[16]
In_2O_3 nanowires	0.5	35	[17]
In_2O_3 nanowires	10	60	[18]
In_2O_3 nanowires	100	200–500	[19]
WO_3 nanowires	0.5	60	[20]
WO_3 nanowires	1	30–200	[21]
SnO_2-core/ZnO-shell nanofibers	1–5	10–40	[22]
MoO_3 lameller	10	118	[23]
TiO_2 nanofibers	100	10,000	[24]

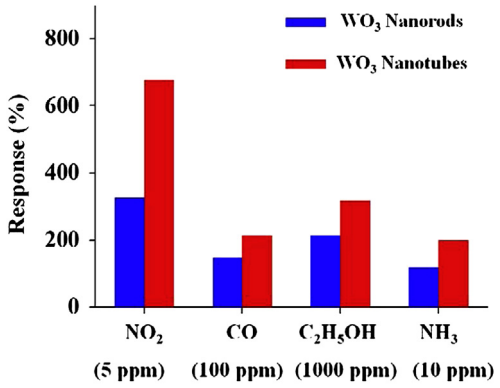

Fig. 7. Comparison of responses of WO_3 nanorods and WO_3 nanotubes to different gases. The results prove that WO_3 nanorods and WO_3 nanotubes have good selectivity for NO_2 gas.

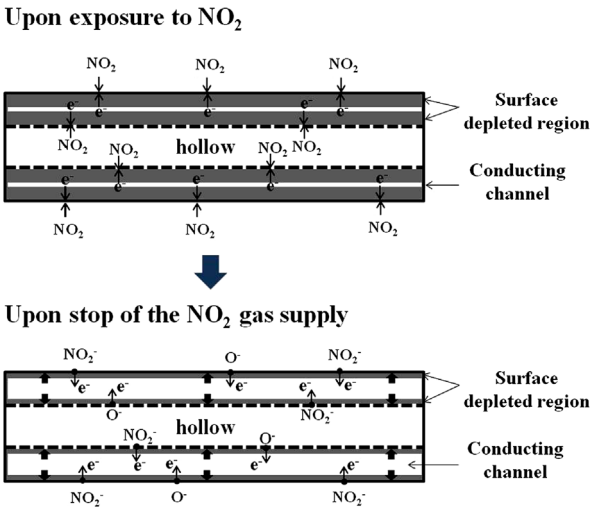

Fig. 8. Schematic diagram showing the width of the depletion region in the WO_3 nanotubes upon exposure to air and NO_2 gas.

4. Conclusions

WO_3 nanotubes were prepared as gas sensors using a TeO_2 nanowire template. The WO_3 nanotube sensor showed responses of 144–1,054% to 1–50 ppm NO_2 at 300 °C. These responses were far superior to those obtained by most oxide one-dimensional nanostructures reported in the literature. The enhanced response of WO_3 nanotubes toward NO_2 gas over that of WO_3 nanorods might be due to the higher surface-to-volume ratio of the WO_3 nanotubes.

Acknowledgment

This work was supported by the Key Research Institute Program′ through the National Research Foundation of Korea (NRF) funded by the Ministry of Education, Science and Technology (2011-0018394).

References

[1] H.H. Tippins, Optical absorption and photoconductivity in the band edge of b-Ga_2O_3, Physical Review A 140 (1965) 316–319.
[2] H. Kim, C. Jin, S. Park, S. Kim, C. Lee, H_2S gas sensing properties of bare and Pd-functionalized CuO nanorods, Sensors and Actuators B 161 (2012) 594–599.
[3] X. Liu, J. Zhang, X. Guo, S. Wu, S. Wang, Enhanced sensor response of Ni-doped SnO_2 hollow spheres, Sensors and Actuators B 152 (2011) 162–167.
[4] M.M. Arsfat, B. Dinan, S.A. Akbar, A.S.M.A. Haseeb, Gas sensors based on one dimensional nanostructured metal-oxides: a review, Sensors 12 (2012) 7207–7258.
[5] S.R. Utembe, G.M. Hansford, M.G. Sanderson, R.A. Freshwater, K.F.E. Pratt, D.E. Williams, R.A. Cox, R.L. Jones, An ozone monitoring instrument based on the tungsten trioxide (WO_3) semiconductor, Sensors and Actuators B 114 (2006) 507–512.
[6] H. Xia, Y. Wang, F. Kong, S. Wang, B. Zhu, X. Guo, J. Zhang, Y. Wang, S. Wu, Au-doped WO_3-based sensor for NO_2 detection at low, operating temperature, Sensors and Actuators B 134 (2008) 133–139.
[7] J. Zhang, X. Liu, M. Xu, X. Guo, S. Wu, S. Zhang, S. Wang, Pt clusters supported on WO_3 for ethanol detection, Sensors and Actuators B 147 (2010) 185–190.
[8] C.S. Rout, G.U. Kulkarni, C.N.R. Rao, Room temperature hydrogen and hydrocarbon sensors based on single nanowires of metal oxides, Journal of Physics D: Applied Physics 40 (2007) 2777–2782.
[9] C.L. Dai, M.C. Liu, F.S. Chen, C.C. Wu, M.W. Chang, A nanowire WO_3 humidity sensor integrated with micro-heater and inverting amplifier circuit on chip manufactured using CMOS-MEMS technique, Sensors and Actuators B 123 (2007) 896–901.
[10] L.F. Zhu, J.C. She, J.Y. Luo, S.Z. Deng, J. Chen, N.S. Xu, Study of physical and chemical processes of H_2 sensing of Pt-coated WO_3 nanowire films, Journal of Physical Chemistry C 114 (2010) 15504–15509.
[11] N.V. Hieu, V.V. Quang, N.D. Hoa, D. Kim, Preparing large-scale WO_3 nanowire-like structure for high sensitivity NH_3 gas sensor through a simple route, Current Applied Physics 11 (2011) 657–661.
[12] S. An, S. Park, H. Ko, C. Lee, Enhanced NO_2 gas sensing properties of WO_3 nanorods encapsulated with ZnO, Applied Physics A 108 (2012) 53–58.
[13] R.A. Gerlitz, K.D. Benkstein, D.L. Lahr, J.L. Hertz, C.B. Montgomery, J.E. Bonevich, S. Semancik, M.J. Tarlov, Fabrication and gas sensing performance of parallel assemblies of metal oxide nanotubes supported by porous aluminum oxide membranes, Sensors and Actuators B 136 (2009) 257–264.
[14] D.E. Williams, Solid State Gas Sensors, Hilger, Bristol, 1987.
[15] E. Oh, H.Y. Choi, S.H. Jung, S. Cho, J.C. Kim, K.H. Lee, S.W. Kang, J. Kim, J.Y. Yun, S.H. Jeong, High-performance NO_2 gas sensor based on ZnO nanorod grown by ultrasonic irradiation high-performance NO_2 gas sensor based on ZnO nanorod grown by ultrasonic irradiation, Sensors and Actuators B 141 (2009) 239–243.
[16] J. Kaur, R. Kumar, M.C. Bhatnagar, Effect of indium-doped SnO_2 nanoparticles on NO_2 gas sensing properties, Sensors and Actuators B 126 (2007) 478–484.
[17] A. Vomiero, S. Bianchi, E. Comini, G. Faglia, M. Ferroni, G. Sberveglieri, Controlled growth and sensing properties of In_2O_3 nanowires, Crystal Growth & Design 7 (2007) 2500–2504.
[18] C.S. Rout, K. Ganesh, A. Govindaraj, C.N.R. Rao, Sensors for the nitrogen oxides, NO_2, NO and N_2O, based on In_2O_3 and WO_3 nanowires, Applied Physics A 85 (2006) 241–246.
[19] C. Li, D. Zhang, X. Liu, S. Han, T. Tang, J. Han, C. Zhou, In_2O_3 nanowires as chemical sensors, Applied Physics Letters 82 (2003) 1613–1615.
[20] D. Zhang, Z. Liu, C. Li, T. Tang, X. Liu, S. Han, B. Lei, C. Zhou, Detection of NO_2 down to ppb levels using individual and multiple In_2O_3 nanowire devices, Nano Letters 4 (2004) 1919–1924.
[21] Z. Liu, M. Miyauchi, T. Yamazaki, Y. Shen, Facile synthesis and NO_2 gas sensing of tungsten oxide nanorods assembled microspheres, Sensors and Actuators B 140 (2009) 514–519.

[22] S.W. Choi, J.Y. Park, S.S. Kim, Synthesis of SnO_2–ZnO core–shell nanofibers via a novel two-step process and their gas sensing properties, Nanotechnology 20 (2009) 465603–465608.

[23] M.B. Rahmani, S. Keshmiri, J. Yu, A. Sadek, L. Al-Mashat, A. Moafi, K. Latham, Y. Li, W. Wlodarski, K. Kalantar-Zadeh, Gas sensing properties of thermally evaporated lamellar MoO_3, Sensors and Actuators B: Chemical 145 (2010) 13–19.

[24] O. Landau, A. Rothschild, E. Zussman, Processing–microstructure–properties correlation of ultrasensitive gas sensors produced by electrospinning, Chemistry of Materials 21 (2009) 9–11.

[25] K.D. Schierbaum, U. Weimar, W. Goepel, R. Kowalkowski, Conductance, work function and catalytic activity of SnO_2-based gas sensors, Sensors and Actuators B 3 (1991) 205–214.

[26] O.V. Safonova, G. Delabouglise, B. Chenevier, A.M. Gaskov, M. Labeau, Co and NO_2 gas sensitivity of nanocrystalline tin dioxide thin films doped with Pd, Ru and Rh, Materials Science and Engineering C 21 (2002) 105–111.